Supplementary Information of "Enhancing luminescence performance of LED-pumped Mn^{4+}-activated highly efficient double perovskite phosphor with A-site defects via local lattice tuning"

Liang Li[1], Qianwen Cao[1], Jing Xie[1], Wenming Wang[1], Hongmei Chen[1], Yubei Wang[1], Zhongyuan Li[2], Yan Pan[3*], Xiantao Wei[4*], Yong Li[1*]

1. *School of Mathematics and Physics, Anhui University of Technology, Maanshan 243000, China*
2. *Key Laboratory of Functional Molecular Solids, Ministry of Education and College of Chemistry and Materials Science, Anhui Normal University, Wuhu 241000, PR China*
3. *Analysis and Testing central Facility, Anhui University of Technology, Maanshan 243000, China.*
4. *Physics Experiment Teaching Center, School of Physical Sciences, University of Science and Technology of China, Hefei, 230026, China*

*Email[1]: yongli@ahut.edu.cn; *Email[2]: yanpan@ahut.edu.cn; *Email[3]: wxt@ustc.edu.cn;

Table S1. The cell parameters, refinement factors, and bond distances of the LMTO: 0.4 mol%Mn^{4+} and LMTO: 0.4 mol%Mn^{4+}, 0.2 mol%Ca^{2+} phosphors.

Formula	LMTO:0.4 mol%Mn^{4+}	LMTO:0.4 mol%Mn^{4+}, 0.2mol%Ca^{2+}
crystal system	Monoclinic	Monoclinic
space group	$I_{2/m}$ (12)	$I_{2/m}$ (12)
a (Å)	5.6377	5.6342
B (Å)	5.6293	5.6255
C (Å)	7.9564	7.9486
V (Å^3)	252.51	251.93
α=γ (°)	90	90
β (°)	89.9999	90.0112
R_{wp} (%)	7.47	8.09
R_p (%)	5.78	6.38
χ^2	1.95	2.32
bond distance Ta_1-O_1 (Å) (2)	2.072	2.069
bond distance Ta_1-O_2 (Å) (4)	2.129	2.128
bond distance Ta_1-Ta_1 (Å)	5.6293(3)	5.6255(2)

Table S2. The atomic coordinates, Wyckoff position, and occupancy of the LMTO: 0.4 mol%Mn^{4+} sample.

atom	Wyckoff position	fractional coordinates			occupancy (×100%)	Uiso
		x	*y*	*z*		
La	4i	0.5026	0	0.2530	0.833	0.005
Mg	2a	0	0	0	1.00	0
Ta	2d	0.5	0.5	0	0.996	0
O_1	4i	0.0809	0	0.2460	1.00	0
O_2	8j	0.2395	0.2298	-0.0321	1.00	0
Mn_1	2d	0.5	0.5	0	0.004	0.006

Table S3. Atomic ratios of the LMTO: 3.0 mol%Mn^{4+} samples for theoretical and measured values.

Element (LMTO: 3.0 mol%Mn^{4+})	La	Mg	Ta	O	Mn
Atomic ratio (%)	19.51	10.93	9.92	57.78	1.86
Theoretical ratio (%)	17.24	10.34	10.03	62.07	0.31

Table S4. The atomic coordinates, Wyckoff position, and occupancy of the LMTO: 0.4 mol%Mn^{4+}, 0.2 mol%Ca^{2+} sample.

atom	Wyckoff position	fractional coordinates			occupancy (×100%)	Uiso
		x	*y*	*z*		
La	4i	0.5026	0	0.2530	0.831	0
Mg	2a	0	0	0	1.00	0.002
Ta	2d	0.5	0.5	0	0.996	0
O_1	4i	0.0809	0	0.2460	1.00	0
O_2	8j	0.2395	0.2298	-0.0321	1.00	0.002
Mn_1	2d	0.5	0.5	0	0.004	0
Ca_1	4i	0.5026	0	0.2530	0.002	0.01

Table S5 Internal quantum efficiency and thermal stability of representative Mn^{4+}-activated matrix materials reported in the last three years.

Num.	Matrices material	Internal quantum efficiency (%)	I_{PL420K}/I_{PL273K} (%)	Ref.
	$La_{1.67}MgTaO_6$	72.65	57.23	This work
1	Ba_2LaTaO_6	26.8	5.5	[1]
2	Sr_2InTaO_6	10.15	2.4	[2]
3	Sr_2GdTaO_6	15.27	31.17	[3]
4	Ba_2GdNbO_6	29.7	~35	[4]
5	$BaSrGdNbO_6$	33.6	~42	[4]
6	$BaSrYNbO_6$	34.6	~47	[4]
7	$Ca_{14}Ga_{10}Zn_6O_{35}$	38.0	41.2	[5]
8	Ca_2YSbO_6	62.6	40	[6]
9	Sr_2InSbO_6	22.67	48	[7]
10	$CaMg_2La_2W_2O_{12}$	44	35	[8]

11	Ba_2YTaO_6	41.5	37	[9]
12	Li_4AlSbO_6	54.8	-	[10]
13	$Ca_3Al_4ZnO_{10}$	30	38	[11]
14	Sr_3NaSbO_6	56.2	39.84	[12]
15	$Li_3Mg_2TaO_6$	23	-	[13]
16	$KLaMgWO_6$	43	-	[14]
17	Cs_2NbOF_5	81.7	~18	[15]
18	K_2NaGaF_6	61	71.9	[16]
19	Cs_2KGaF6	80.2	~45	[17]
20	Cs_2SiF_6	69	70	[18]
21	K_2TiF_6	93	30	[18]
22	Na_2SiF_6	70	70	[18]

Table S6. The CIE chromaticity coordinates, CRI, and CCT of the warm wLEDs are prepared by different phosphor ratios.

Ratio	Coordinate	CRI	CCT
Y:R=1:0	(0.2944,0.3264)	76.5	7595 K
Y:R=1:5	(0.3101,0.3305)	80.6	6395 K
Y:R=1:10	(0.3266,0.3313)	84.5	5775 K
Y:R=1:15	(0.3552,0.3582)	86.1	4658 K

Table S7 Lumen efficiency (lm/W) of the wLEDs devices prepared with different ratios. of phosphors at different driving currents.

Ratio	10 mA	20 mA	40 mA	60 mA	100 mA
Y:R=1:0	140.42	129.25	122.22	119.42	112.40
Y:R=1:5	109.99	92.47	80.85	74.72	68.29
Y:R=1:10	85.06	69.06	55.70	51.59	45.01
Y:R=1:15	72.66	57.92	47.30	41.00	36.66

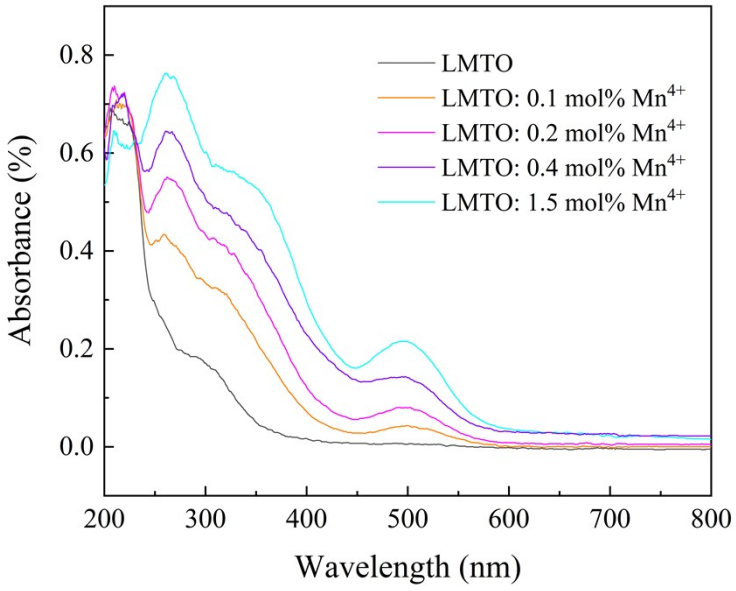

Fig. S1 Absorption spectra of perfect LMTO samples and samples with different Mn^{4+} doping concentrations.

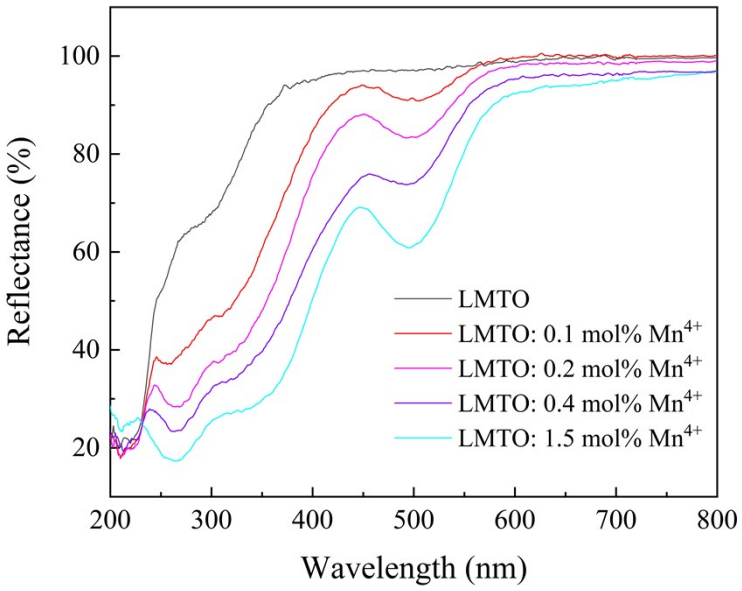

Fig. S2 Diffuse reflectance spectra of perfect LMTO samples and samples with different Mn^{4+} doping concentrations.

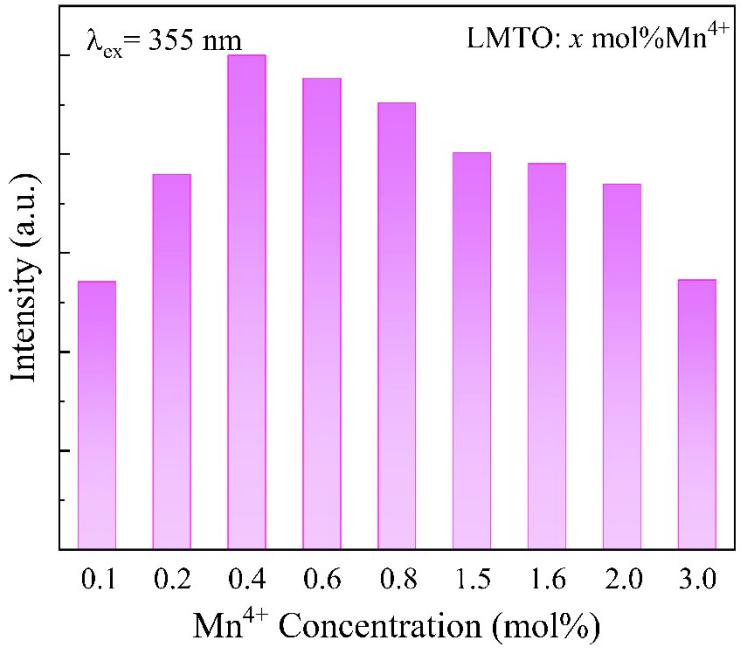

Fig. S3. Histogram of the integrated emission intensity for the LMTO phosphor with different Mn^{4+} ion concentrations.

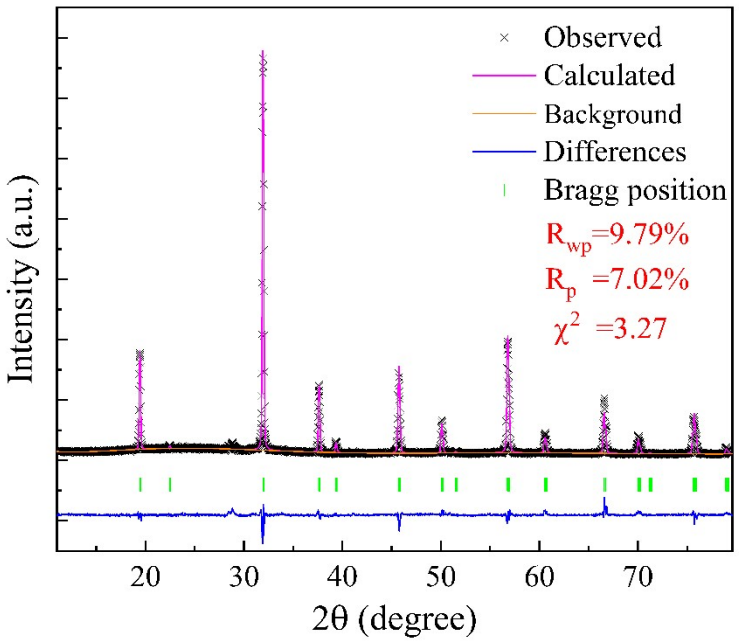

Fig. S4. The Rietveld refined XRD pattern of the sample co-doped with Li^+ ions.

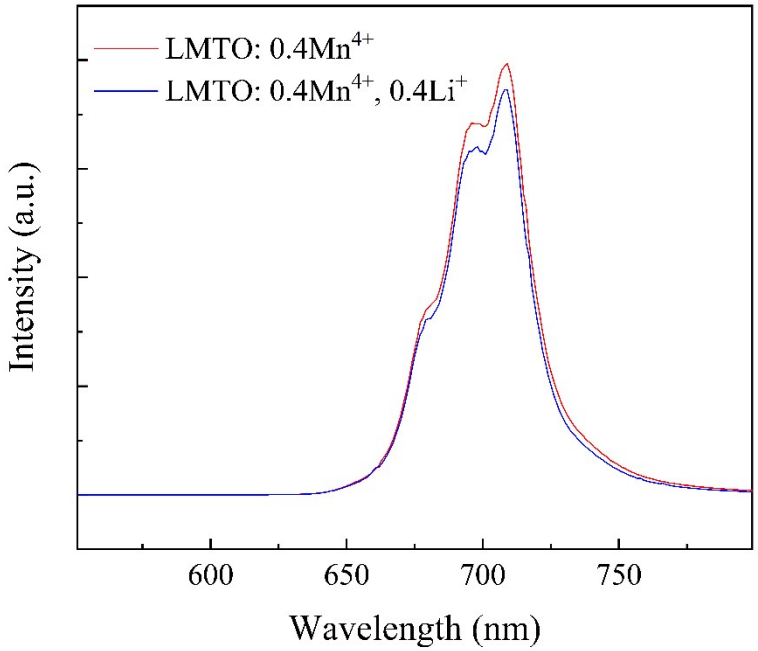

Fig. S5. The PL spectra of the samples doped and without doped Li^+ ions.

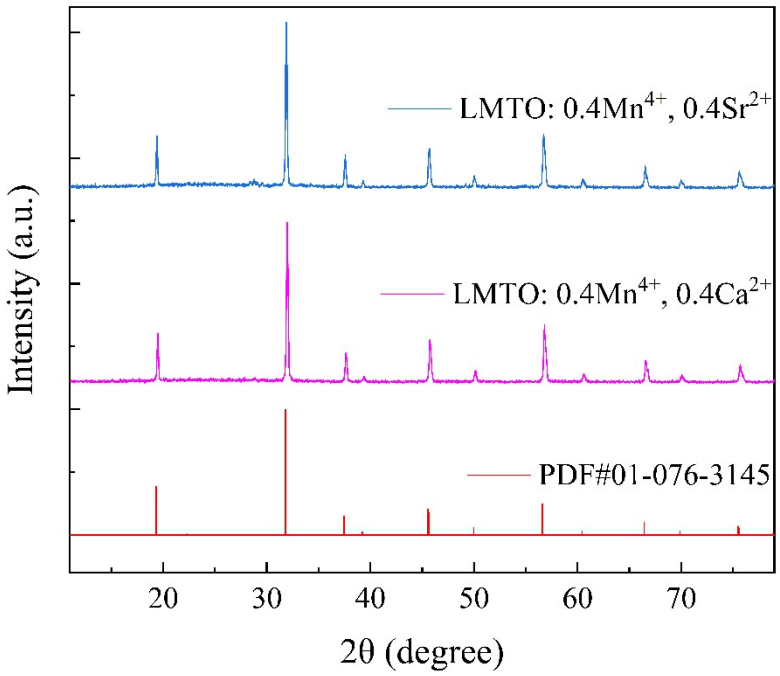

Fig. S6. The XRD curves of samples after co-doping with Ca^{2+} or Sr^{2+} ions and the LMTO compound standard PDF card.

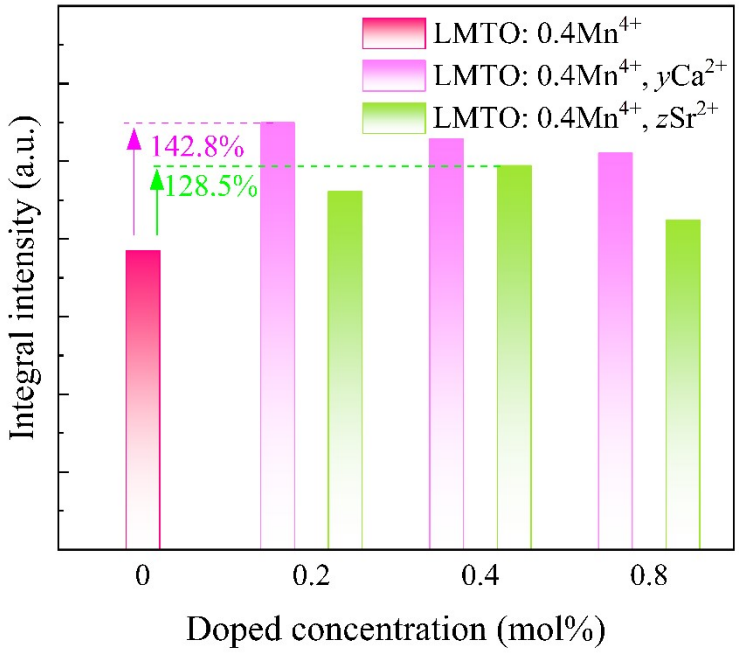

Fig. S7. Histogram of the integrated emission intensity for the samples after co-doping with Ca^{2+} or Sr^{2+} ions.

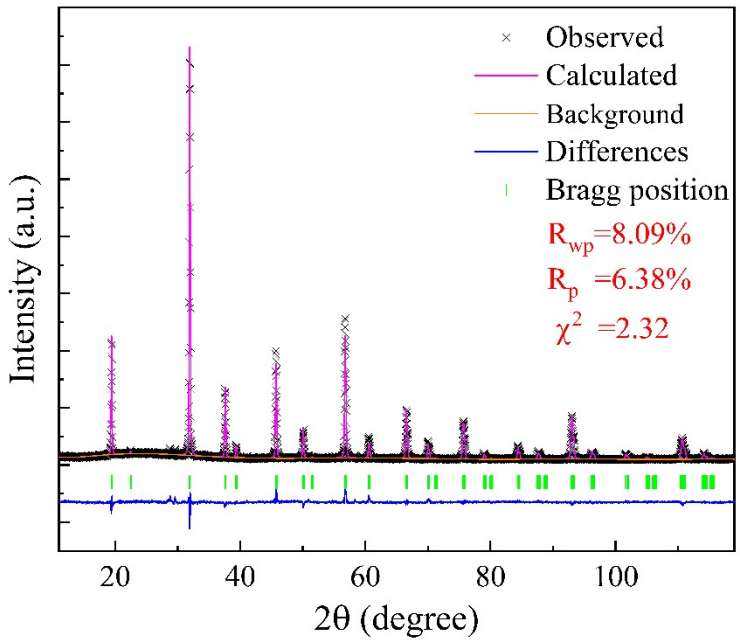

Fig. S8. The XRD pattern after Rietveld refinement of the LMTO: 0.4 mol%Mn^{4+}, 0.2 mol%Ca^{2+} sample.

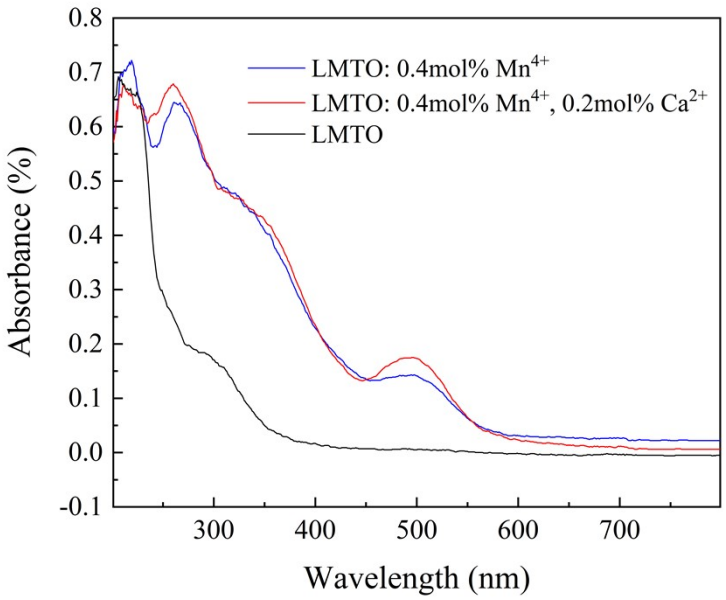

Fig. S9 Absorption spectra of samples with and without Ca^{2+} ions doping.

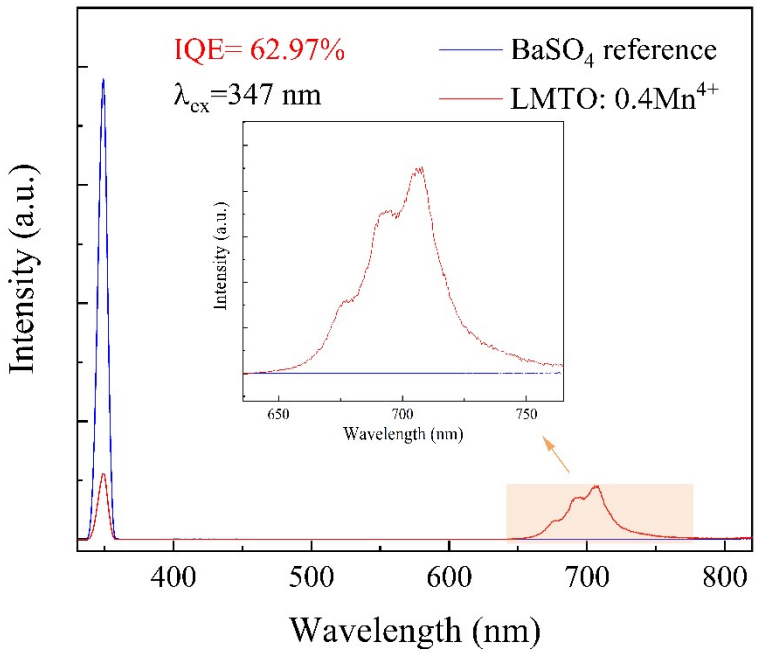

Fig. S10. The IQE of the LMTO: 0.4 mol%Mn^{4+} sample.

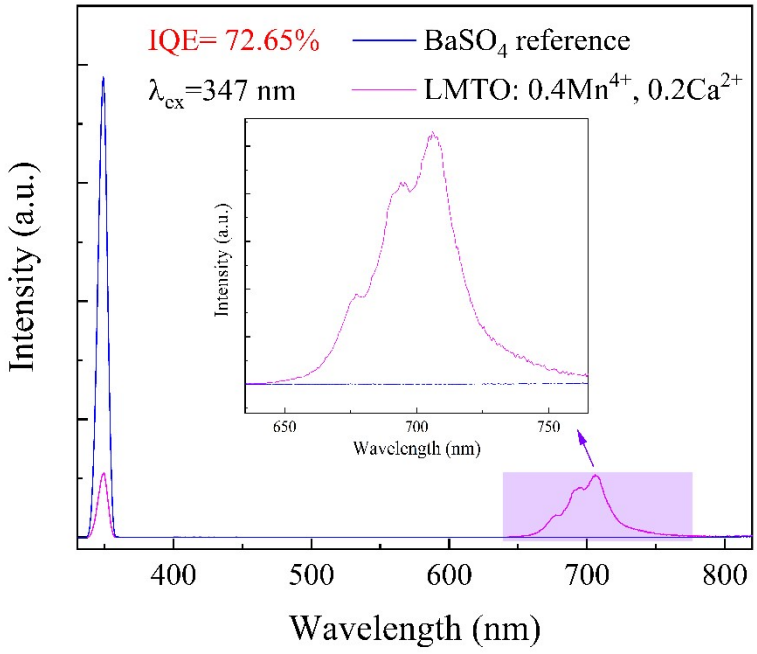

Fig. S11. The IQE of the LMTO: 0.4 mol%Mn^{4+}, 0.2 mol%Ca^{2+} sample.

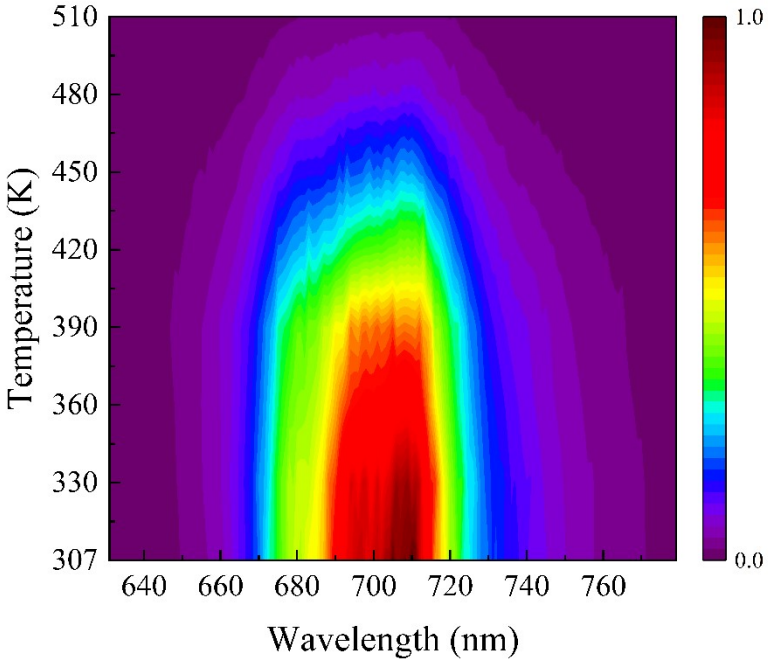

Fig. S12. The two-dimensional contour plot of the PL spectra with temperature for the LMTO: 0.4 mol%Mn^{4+} sample.

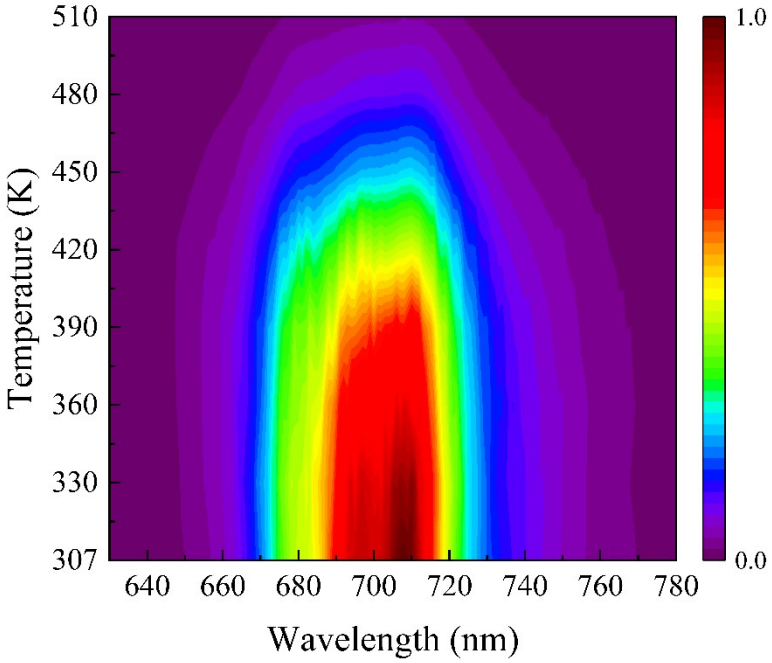

Fig. S13. The two-dimensional contour plot of the PL spectra with temperature for the LMTO: 0.4 mol%Mn^{4+}, 0.2 mol%Ca^{2+} sample.

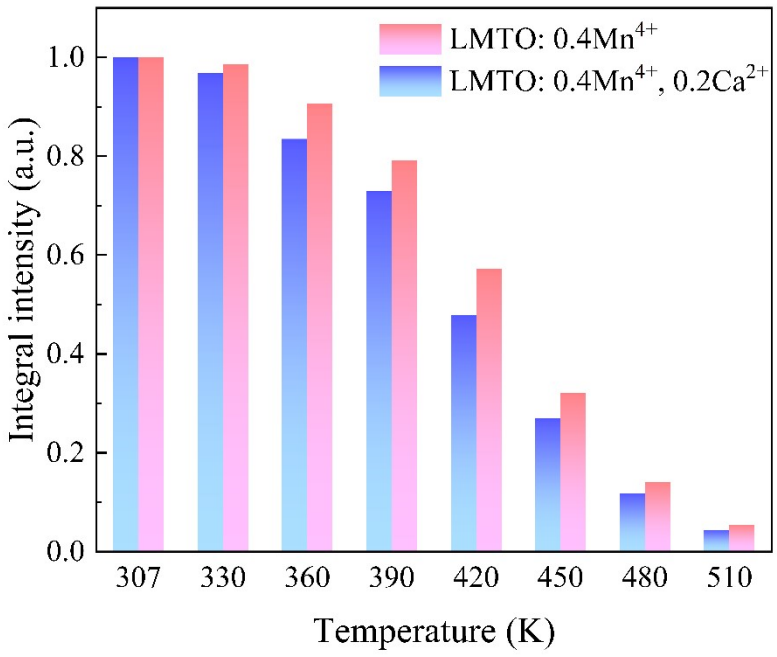

Fig. S14. Histogram of integrated emission intensity at different temperatures for the samples with and without co-doped Ca^{2+} ions.

References

1. L. Li, Q. Cao, J. Wang, Z. Li, Y. Pan, X. Wei and Y. Li, *Ceramics International*, 2022, DOI: https://doi.org/10.1016/j.ceramint.2022.08.170.
2. Q. Cao, L. Li, Y. Wang, W. Wang, H. Chen, Y. Pan, X. Wei and Y. Li, *Journal of Luminescence*, 2022, **252**, 119351.
3. Z. Wu, L. Li, H. Li, L. Mei, W. Xia, Y. Yi and Y. Hua, *Dalton Transactions*, 2022, **51**, 9062-9071.
4. Q. Zhu, M. Li, Y. Jin, Z. Mei, J. Gao, J. Huo and Q. Wang, *Chemical Engineering Journal*, 2021, **424**, 130571.
5. Y. Zhong, S. Gai, M. Xia, S. Gu, Y. Zhang, X. Wu, J. Wang, N. Zhou and Z. Zhou, *Chemical Engineering Journal*, 2019, **374**, 381-391.
6. J. Zhong, D. Chen, X. Chen, K. Wang, X. Li, Y. Zhu and Z. Ji, *Dalton Transactions*, 2018, **47**, 6528-6537.
7. Y. Xie, X. Geng, Y. Wang, J. Guo, Y. Lu, Q. Lv, Z. Ma, D. zhang, J. Zhao, B. Deng and R. Yu, *Journal of the American Ceramic Society*, 2022, **105**, 1300-1317.
8. N. Ma, W. Li, B. Devakumar, Z. Zhang and X. Huang, *Materials Today Chemistry*, 2021, **21**, 100512.
9. W. Li, N. Ma, Q. Sun, S. Wang, Z. Zhang, B. Devakumar and X. Huang, *Journal of Luminescence*, 2020, **228**, 117621.
10. G. Li, G. Liu, Q. Mao, G. Du, X. Li, Y. Zhu, T. Yang, H. Yu, Z. Ji and J. Zhong, *Ceramics International*, 2021, **47**, 27609-27616.
11. L. Sun, B. Devakumar, J. Liang, S. Wang, Q. Sun and X. Huang, *Journal of Alloys and Compounds*, 2019, **785**, 312-319.
12. L. Shi, J.-x. Li, Y.-j. Han, W.-l. Li and Z.-w. Zhang, *Journal of Luminescence*, 2019, **208**, 201-207.

13. S. Wang, Q. Sun, J. Liang, L. Sun, B. Devakumar and X. Huang, *Inorganic Chemistry Communications*, 2020, **116**, 107903.
14. J. Liang, B. Devakumar, L. Sun, Q. Sun, S. Wang, B. Li, D. Chen and X. Huang, *Ceramics International*, 2019, **45**, 4564-4569.
15. J. Zhou, Y. Chen, C. Jiang, B. Milićević, M. S. Molokeev, M. G. Brik, I. A. Bobrikov, J. Yan, J. Li and M. Wu, *Chemical Engineering Journal*, 2021, **405**, 126678.
16. C. Jiang, M. G. Brik, L. Li, L. Li, J. Peng, J. Wu, M. S. Molokeev, K.-L. Wong and M. Peng, *Journal of Materials Chemistry C*, 2018, **6**, 3016-3025.
17. J. Li, Y. Wang, H. Zhe, Y. Zhou, Q. Zhou and Z. Wang, *Journal of Alloys and Compounds*, 2021, **881**, 160624.
18. X. Luo, Z. Hou, T. Zhou and R.-J. Xie, *Journal of the American Ceramic Society*, 2020, **103**, 1018-1026.